Cerebral Cortex January 2012;22:60–73
doi:10.1093/cercor/bhr072
Advance Access publication May 12, 2011

# Long-Range Clustered Connections within Extrastriate Visual Area V5/MT of the Rhesus Macaque

Bashir Ahmed, Patricia M. Cordery, Douglas McLelland, Wyeth Bair and Kristine Krug

Department of Physiology, Anatomy and Genetics, University of Oxford, Oxford OX1 3PT, UK

Address correspondence to Dr Kristine Krug, Department of Physiology, Anatomy and Genetics, University of Oxford, Sherrington Building, Oxford OX1 3PT, UK. Email kristine.krug@dpag.ox.ac.uk.



**Visual area V5/MT in the rhesus macaque has a distinct functional organization, where neurons with specific preferences for direction of motion and binocular disparity are co-organized in columns or clusters. Here, we analyze the pattern of intrinsic connectivity within cortical area V5/MT in both parasagittal sections of the intact brain and tangential sections from flatmounted cortex using small injections of the retrograde tracer cholera toxin subunit b. Labeled cells were predominantly found in cortical layers 2, 3, and 6. Going along the cortical layers, labeled cells were concentrated in regularly spaced clusters. The clusters nearest to the injection site were approximately 2 mm from its center. In flatmounted cortex, along the dorsoventral axis of V5/MT, we identified further clusters of labeled cells up to 10 mm from the injection site. Quantitative analysis of parasagittal sections estimated average cluster spacing at 2.2 mm; in cortical flatmounts, spacing was 2.3 mm measured radially from the injection site. The results suggest a regular pattern of intrinsic connectivity within V5/MT, which is consistent with connectivity between sites with a common preference for both direction of motion and binocular depth. The long-range connections can potentially account for the large suppressive surrounds of V5/MT neurons.**

**Keywords:** column, connectivity, cortex, horizontal, monkey

## Introduction

In primary visual cortex (V1), columnar organization is associated with specific long-range horizontal connections (Gilbert and Wiesel 1989; Bosking et al. 1997; Sincich and Blasdel 2001). These connections make an identifiable functional contribution to the receptive field (RF) of V1 neurons (Angelucci, Levitt, et al. 2002). Like V1, extrastriate visual area V5/MT of the macaque monkey has a distinct functional organization. The predominant functional characteristic of neurons in V5/MT is their direction selectivity independent of stimulus shape (Dubner and Zeki 1971; Zeki 1974b; Maunsell and Van Essen 1983b). They show tuning for speed of motion (Cheng et al. 1994) and some show selectivity for the direction of visual patterns (Movshon et al. 1983; Albright 1984). Many V5/MT neurons are tuned to binocular disparity as well as motion direction (Zeki 1974a; Maunsell and Van Essen 1983a). The RFs of these neurons also have large suppressive surrounds (Tanaka et al. 1986). Based on shape and distribution of the surrounds, it has been suggested that horizontal connections from within V5/MT provide the input for the surrounds (Raiguel et al. 1995).

Systematic neurophysiological recordings within V5/MT by Albright et al. (1984) have strongly suggested a columnar organization for direction of motion (see also Zeki 1974b). The motion direction preferred by each column of neurons shifts gradually across the cortical surface but changes little orthogonal to the cortical layers; it has been estimated that a single 360° cycle of motion directions is encountered over 1 mm of cortex when moving an electrode parallel to the layers. In support of this finding, 2-deoxyglucose studies of V5/MT have confirmed a patchy arrangement of cortical label for narrowband directional stimuli (Geesaman et al. 1997). Independent of this organization for direction of motion, electrophysiological studies have found a clustered organization for binocular disparity in V5/MT (DeAngelis and Newsome 1999). Lesion studies, neurophysiological recordings, and electrical microstimulation in the monkey have linked neuronal activity in V5/MT directly to perception of both visual motion and binocular depth (Newsome and Pare 1988; Newsome et al. 1989; Salzman et al. 1990; Marcar and Cowey 1992; DeAngelis et al. 1998; Krug et al. 2004).

While intercortical and subcortical connections to and from V5/MT have been extensively studied in the macaque monkey, the pattern of intrinsic connectivity within V5/MT is not well understood. In a New World species, the owl monkey, Weller et al. (1984) found that injections of the anterograde tracer $^{3}$H-proline into MT labeled about 6 alternating bands, which ran perpendicular to the cortical surface through the layers in coronal sections. Using biocytin injections in flattened cortex of the same species, Malach et al. (1997) reported horizontal connections organized into bands. The average separation from the injection center to the furthest patch was approximately 1.8 mm. More widespread intrinsic connectivity has been suggested for the Old World macaque monkey, but the results were inconsistent between the 3 animals in that study (Maunsell and Van Essen 1983c).

While many neurons in V5/MT of the owl monkey are tuned to direction of motion, the functional organization between Old and New World Monkeys might differ. In the owl monkey, selectivity for binocular disparity seems rare (Zeki 1980; Felleman and Kaas 1984); evidence for columns of opposite direction preference has been found (Malonek et al. 1994). In the rhesus macaque, the pattern of inputs from area V1 and V2 to V5/MT provides an indication of a columnar architecture within V5/MT (Rockland 2002). Injections of anterograde tracers in V1 have been reported to label clusters about 1–2 mm in size in V5/MT, with an intercluster spacing of about 2–3 mm (Van Essen et al. 1981). Individual axons originating from V1 or V2 terminate in a patchy manner over a wide territory in V5/MT. Well-defined individual axonal arbor terminations have a width of typically 200 μm (Rockland 1989, 1995).

In this study, we examined the intrinsic circuitry of V5/MT in the macaque monkey with small volume injections of the retrograde tracer cholera toxin subunit b (CTb), following

characterization of the local response properties of cells. We analyzed the pattern of retrogradely labeled cells 1) on parasagittal sections across layers 1–6 in the long dorsoventral axis of V5/MT and 2) in whole brain flatmounts within layers 2–5. We quantified the pattern of label to assess regularities in the spatial organization of intrinsic connectivity. To our knowledge, this is the first systematic study of the intrinsic connectivity within extrastriate visual area V5/MT in the rhesus macaque.

## Methods

### *Animals and Anesthesia*

Seven adult rhesus macaques, weight range 3.2–17.0 kg, were used in this study (6 male and 1 female). They were initially given an intramuscular (i.m.) injection of a mixture of ketamine HCl (10 mg/kg) and Midazolam (Hypnovel, 0.1 mg/kg). To mitigate the bradycardia induced by Midazolam, an i.m. injection of Atropine Sulphate (0.05 mg/kg) was also given. Local anesthetic was applied to the outer ear canal (Emla cream 5%, lidocaine:prilocaine 1:1), and Lidocaine HCl spray (Intubeaze 2%) was applied to the region around the oropharynx. Animals were intubated with an appropriately sized (3–5.5 mm internal diameter) endotracheal cannula, and the head was placed in stereotaxic coordinates within a stereotaxic frame. The animals were artificially ventilated (0.5–2.0% Isoflurane in a mixture of 50%:50% $O_2$:air) to maintain end-tidal $CO_2$ to 38 mm Hg. During the maintenance phase, a regime of 100% air would have been equally feasible. Electrocardiogram and heart rate, oximetry, body temperature, noninvasive blood pressure (BP) (in 3 of 7 animals also arterial BP), and electroencephalography were continuously monitored. The left and right saphenous veins were cannulated (BP Venflo intravenously [i.v.] cannula, 0.8 × 25 mm). The anesthetic regime was modified to provide a continuous i.v. infusion of Sufentanil Citrate (loading dose 0.03 μg/kg, continuous infusion at 0.6 μg/kg/h) and Isoflurane (~0.5%) and the animal prepared for aseptic surgery. Craniotomies (diameter 12 mm, overlying the visual cortex) were centered at lateral 16.5 mm from the midline and posterior 20 mm from ear bar zero. A durotomy, 2–4 mm in diameter, was centered at lateral 16 mm and 8 mm posterior to the lunate sulcus. A sterile plastic chamber was attached to the bone around the craniotomy with wax (Tacky wax). A single suture was inserted into the upper eyelids to hold the eyelids open. Following completion of surgical procedures, the animals were paralyzed by an intravenous infusion of vecuronium bromide (Norcuron, 0.1 mg/kg/h). The eyes were fitted with +3 Diopter contact lenses, checked retinoscopically to focus them to the monitor screen at 1.14 m by addition of spherical lenses. The right and left foveae were back projected and the monitor placed appropriately at this location to cover the contralateral visual field for the hemisphere that was recorded. Daily, the animals were massaged, the bladder checked every 12 h and emptied manually if required, and animas were given i.v. methylprednisolone (Solu-Medrone injection, slowly over 2 min at a dose of 10 mg/kg). All procedures conformed to United Kingdom Home Office regulations on animal experimentation and to the European Communities Council Directive of 24 November 1986 (86/609/EEC).

### *Recording*

We recorded neuronal activity with a tungsten electrode (Microprobe Inc., impedance 0.6–1.2 MOhms) attached to a glass capillary with internal tip diameters between 8 and 25 μm (Plowden and Thompson Ltd, outer diameter 0.9 mm, internal diameter 0.12 or 0.22 mm; Fig. 1*A*) and containing the tracer, CTb (1% low salt solution in double distilled $H_2O$, List Biological Laboratories Inc.). The electrode assembly was introduced into the visual cortex at an angle of 20° to the horizontal plane at coordinates 15–17 mm lateral to the midline and 5.5–8 mm posterior to the lunate sulcus. The assembly was inserted 1–1.5 mm into visual cortex under coarse control and then advanced in 2–20 μm steps via a stepper motor system (Narishige). Signals were preamplified

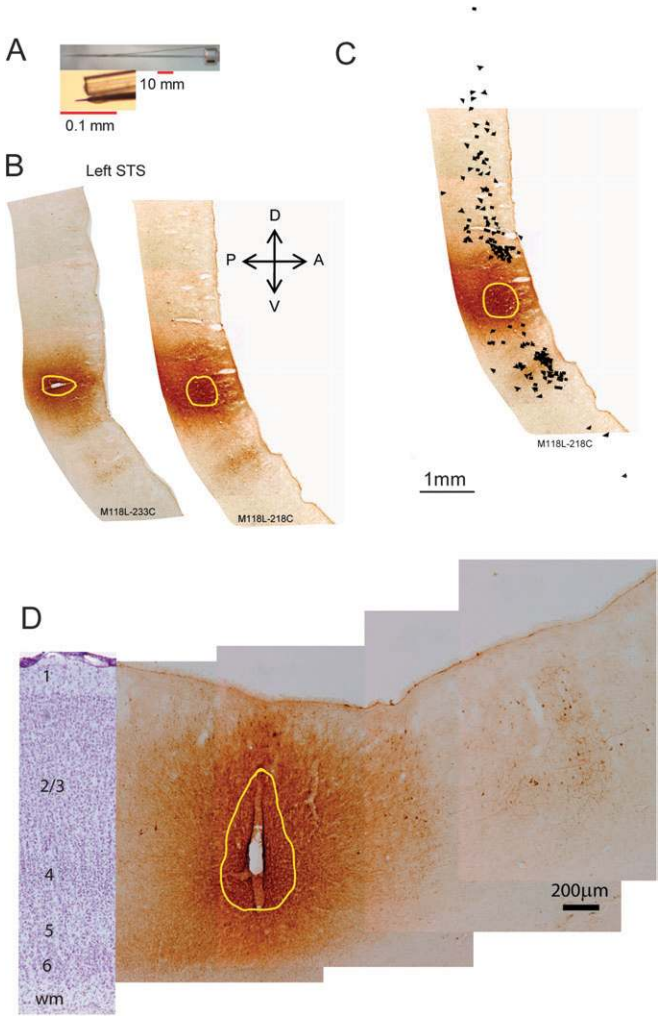


**Figure 1.** CTb injections and label within parasagittal section. (*A*) Dimensions of the electrode assembly consisting of a tungsten recording electrode attached to a glass capillary tube. The glass capillary tube had an outer diameter of 0.9 mm and internal diameter of either 0.22 or 0.12 mm, giving an ejection volume of, respectively, 40 or 10 nL/mm length of capillary. The pulled tip lengths varied from 6 to 16 mm, and the final pore diameter at the tip was set to values from 8 to 25 μm. (*B*) Two parasagittal sections showing the posterior bank of the STS. The 2 sections were separated by 750 μm mediolaterally and the darkly labeled CTb injection site spans both sections. Ventral to the injection site are, in both sections, areas with a higher density of labeled cells, which appear as clusters in the superficial layers 2–4. A, anterior; P, posterior; D, dorsal; V, ventral. (*C*) The right section from (*B*), this time shown with the Neurolucida record of the CTb labeled cells that were identified under higher magnification superimposed onto the section. (*D*) Injection site and cluster of retrogradely labeled cell bodies from (*B*) (left) at higher magnification. The aligned, representative section of Nissl-stained V5/MT shows that the core of the injection site spans layers 2–4. Darkly stained cell bodies with the typical internal structure of CTb label are visible in a cluster to the right. Yellow circle indicates location of the injection site core.

(Dagan extracellular head stage, filter setting 30 Hz, gain ×100), amplified (via Dagan BVC-700A and TREC, filter setting 0.5–2 kHz, gain ×500), and digitized (12.5 kHz). We plotted the minimum response field under computer control with a bar, sine-wave grating or array of dots. We characterized the multi or single units systematically by presenting a series of drifting sinusoidal gratings (on a CRT at a refresh rate of 96 Hz, mean luminance 27 cd/$m^2$) to generate tuning curves for direction, spatial frequency, temporal frequency, and size.

### *Tracer Injection*

In order to verify that we had reached cortical area V5/MT, we used a set of well-established criteria:

1. We noted the extent and sequence of gray matter and white matter along the penetration on approach to V5/MT.
2. We measured the depth of the penetration from the cortical surface.
3. To identify V5/MT, we checked at regular intervals for direction selectivity that was consistent across units at a recording site.
4. We expected to observe smooth changes in the preferred direction of motion when the electrode was moved through putative area V5/MT.
5. We also made use of the established relationship between eccentricity and RF size in V5/MT (Albright and Desimone 1987).
6. If we made more than one penetration, we also checked whether the RF position shifted in location as expected from the topographic map.

The electrode approached V5/MT posteriorly, entering first layer 6. Tracer injections were placed at varying depths, up to 1.6 mm, into V5/MT at locations where we had neurophysiologically characterized the responses. We pressure injected between 10 and 80 nL of CTb (low salt, List Biological Laboratories Inc.). After 48–72 h, animals were perfused and the tissue processed. In some animals, we made injections into both hemispheres. We had investigated callosal transport of CTb tracer in an earlier experiment where we only injected one hemisphere. In one animal, we sectioned and reacted the uninjected hemisphere and found no callosal transport into V5/MT of this hemisphere. Injection site size was measured in the histological sections. The effective tracer uptake zone for CTb was defined as the darkest region at the center of the injection site where no labeled cell bodies or fibers could be discerned under high magnification (Jeffs et al. 2009).

### *Histology*

Four hemispheres from 4 animals were cut parasagittally after tissue was fixed with 4% paraformaldehyde in 0.1 M phosphate buffer and cryoprotected in 10%, 20%, and, finally, 30% sucrose with 4% paraformaldehyde in 0.1 M phosphate buffer. The tissue was sectioned on a freezing stage microtome at 50 μm. V5/MT boundaries were confirmed by staining a one-in-five series of sections with SMI-32 antibody (mono-neurofilament H, nonphosphorylated, ascites, Covance Research Products) and/or myelin stain (Gallyas 1979) (Figs 2 and 3*B*). A one-in-five series of sections were reacted and histologically examined for CTb labeled cells, and another series was Nissl stained.

After perfusion with 1% paraformaldehyde, the cortex from 3 animals (5 hemispheres) was flatmounted, followed by postfixation and cryoprotection (as described in detail by Sincich et al. 2003). A one-in-two or one-in-three series of tangential sections (thickness 70 μm) was reacted for CTb. Sections of 70 μm were required because the large whole hemisphere flatmounts are quite fragile. To allow optimal penetration of antibodies and reagents, sections were reacted free floating. Alternate sections were reacted for cytochrome oxidase (adapted from Wong-Riley 1979) to identify boundaries of V5/MT (Sincich et al. 2003). The outlines of the fiducial features in the sections were also traced (e.g., in parasagittal sections, the boundary defining the superior temporal sulcus (STS); magnification ×1.6).

The centers of CTb labeled cells were marked, defining their location and depth (magnification ×10 or ×20) with the use of Neurolucida (Microbrightfield Ltd). CTb labeled cell bodies were identified under high magnification based on their distinct intrinsic pattern of label.

#### *CTb Immunocytochemistry*

Sections were either reacted immediately or stored in an antifreeze solution at –20 °C. The staining protocol was as follows: sections were washed and treated for endogenous peroxidase, incubated in a blocking buffer to block nonspecific sites, incubated in primary antibody (goat anti-cholera toxin b subunit) diluted 1:8000–1:10 000 for 16–20 h at 4 °C. Secondary antibody (biotinylated rabbit anti-goat IgG, Vector Labs) diluted 1:300 for 90 min at room temperature (RT) followed by ABC (Vector Elite) for 60 min at RT. Finally, sections were reacted with SigmaFast™ DAB for 4–5 min at RT to produce a visible end product. Sections were mounted onto slides, air-dried, dehydrated, and cover-slipped with DPX (Merck).

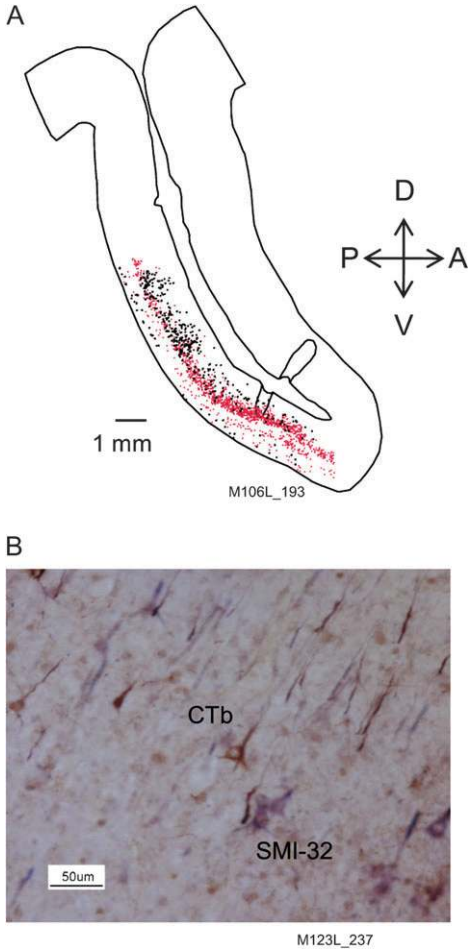


**Figure 2.** The pattern of intrinsic connectivity differed across the layers. (*A*) Neurolucida drawing of cells labeled retrogradely with CTb (black) or stained with antibody SMI-32 (red). In V5/MT, SMI-32 labels pyramidal cells in layers 3 and 5, while the CTb injection predominantly labeled cells in layers 2, 3, and 6. The band of SMI-32 labeled cells in layer 5 highlights the absence of CTb labeled cells in this layer and at least part of layer 4. A, anterior; P, posterior; D, dorsal; V, ventral. (*B*) At higher magnification, CTb and SMI-32 labeled cells display a distinct pattern and color of label that can be readily distinguished. The brown/black CTb label formed a distinct punctate type feature in cell bodies with usually a less dense central zone. The purple SMI-32 label formed a homogeneous label throughout the cell body and its dendrites.

#### *CTb and SMI-32 Double Labeling*

This protocol was undertaken for at least one series of parasagittal sections for each animal to determine the layers within V5/MT that had CTb labeled cells and the injection site. For this protocol, a cocktail of primary antisera for CTb (1:10 000) and SMI-32 (1:5000) was used. The tissue was then processed as above for CTb label, then incubated in secondary antibody against the SMI-32 primary antibody (biotinylated horse anti-mouse IgG, Vector Labs), followed by an ABC (Vector Elite) and developed with Vector VIP (Vector Labs), to give a contrasting purple colored label to SMI-32-positive cells (Fig. 2*B*), typically found in cortical layers 3 and 5 of V5/MT.

### *Geometric Analysis of Labeled Cells*

We quantitatively analyzed the positions of labeled cells within V5/MT, which we had drawn in Neurolucida, in 3 ways.

#### *1. Fourier Analysis*

For each parasagittal section of a one-in-five series across the mediolateral extent of V5/MT, a linear to higher degree polynomial regression curve was fitted by optimizing the adjusted $r^2$ value with the

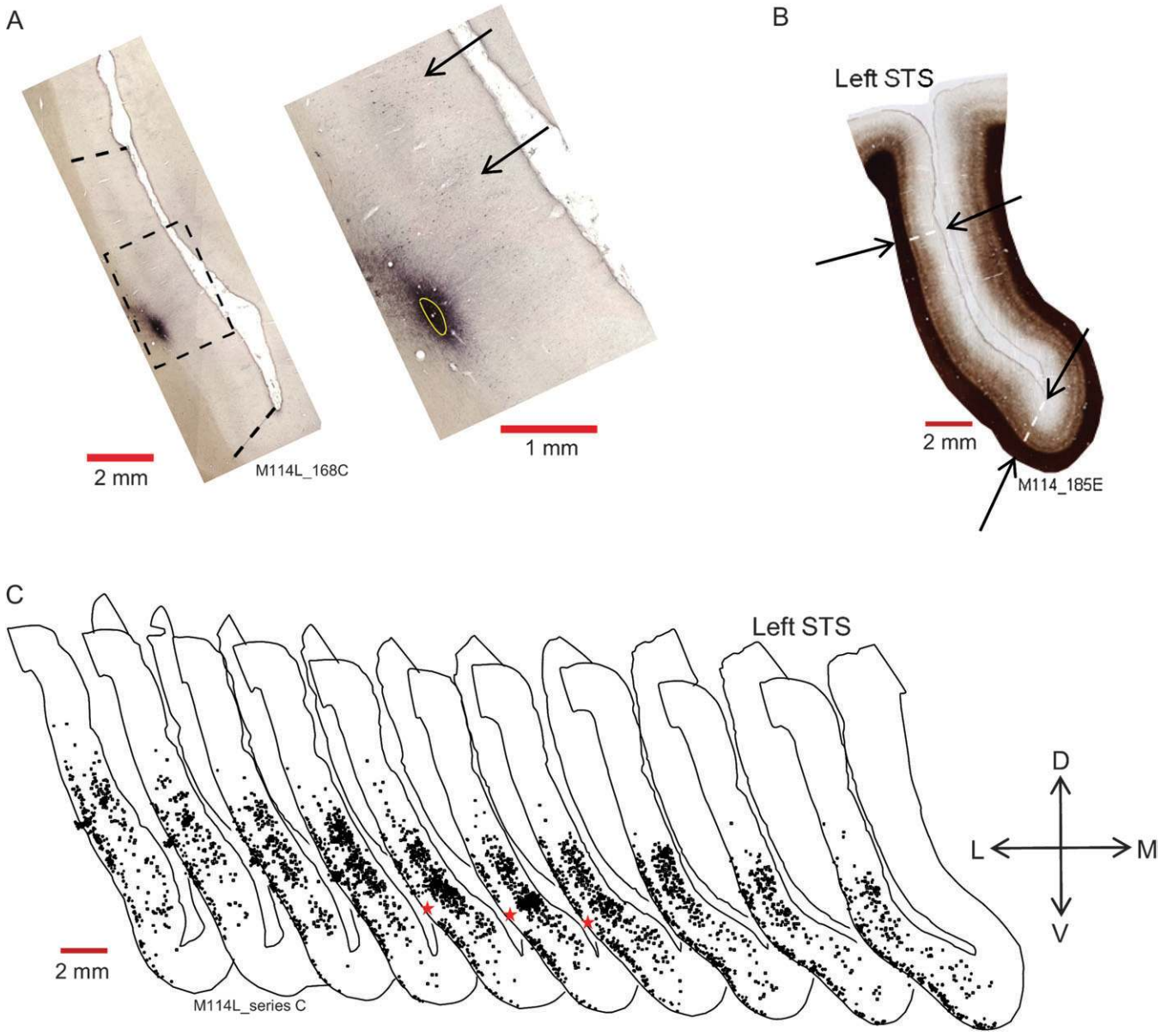


**Figure 3.** Pattern of horizontal connectivity across V5/MT. (*A*) Photomontage of a parasagittal section through the left STS from one animal. The injection site (dense region of black label) was localized to the deep layers of V5/MT on the posterior bank. Injection site and retrogradely labeled CTb cells within the dashed rectangular region are shown to the right. Arrows point to clusters of labeled cells. Yellow circle indicates location of the injection site core. (*B*) A photomontage of a nearby parasagittal section stained for myelin (Gallyas). The transitions from the dense area of label on the posterior bank of the STS to more lightly stained areas demarcate the dorsal and ventral borders of V5/MT (dashed white lines, black arrows). (*C*) A one-in-five series of sections through V5/MT from the same left cortical hemisphere drawn with Neurolucida. Sections are 250 μm apart and run from lateral to medial. For each section, the outline of the STS region was drawn with labeled cells denoted as dots. The injection site was localized to layers 5 and 6 (red star). Cells were retrogradely labeled throughout V5/MT in layers 2–3 and 6 with a clear gap around layers 4–5. Although labeled cells were found spread along the layers, clusters of higher density of labeled cells were apparent. A, anterior; P, posterior; D, dorsal; V, ventral.

curve-fitting function "cftool" in Matlab. This was undertaken for the cell positions within layer 6 separately from those in layers 2–4. The regression lines ran approximately parallel to the layers (Fig. 4*A*). The projection of these cells onto the regression line revealed the variation of density along V5/MT's dorsoventral axis. To linearize the curved polynomial fitted line, a length analysis at 0.5-μm step size was carried out between the minimum and maximum data points. We derived the primary modulation frequency from this density profile with Fourier analysis (F1 component), which provided an estimate of the distance between high-density labeled regions (clusters), that is, the cluster spacing. For the analysis, injection sites were treated as high-density areas of labeled cells. Thus, they contributed to the F1 component. We also extracted the amplitude of the F0 component to assess background labeling. This was compared with the peak densities derived from the density histogram of the labeled cells projected onto the fitted line.

*2. K*-means Cluster Analysis

K-means analysis (Matlab, "kmeans") was applied to the pattern of labeled cells for each parasagittal section of a one-in-five series across the mediolateral extent of V5/MT. The algorithm is an iterative procedure that assigns each data point to the cluster whose center is the nearest. The algorithm requires the number of clusters to be preset. The final best fit to our data was taken as the one with the lowest total sum of distances over all replicates and with the highest average silhouette value (a measure of how close each point in one cluster is to

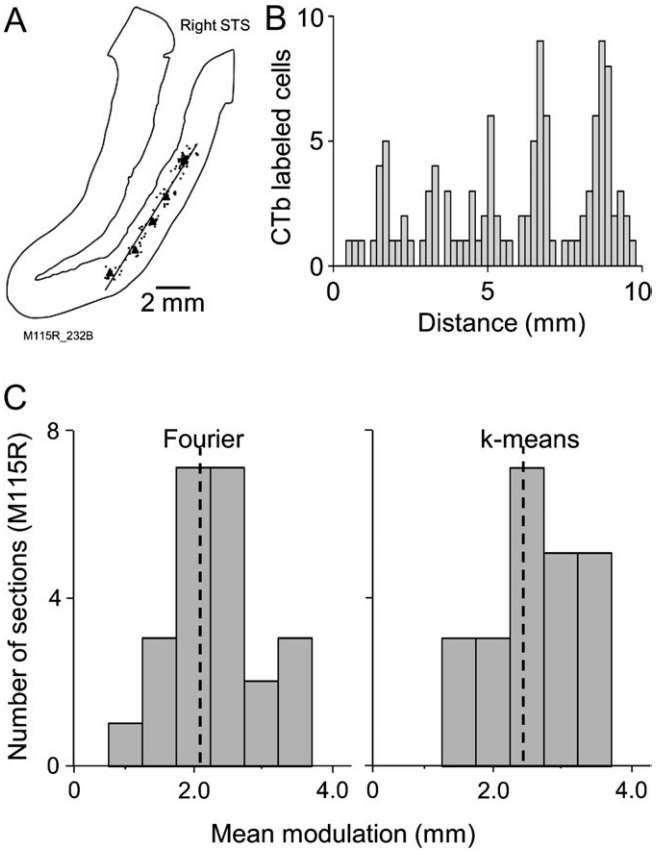


**Figure 4.** Fourier analysis of the pattern of labeled cells. (*A*) The outline of the STS on a parasagittal section is shown with dots representing CTb labeled cells in the superficial layers. The best fit in this example was linear; the regression line has been drawn through the labeled cell locations. Cells were projected onto the line for Fourier analysis. Independently determined locations of cluster centers with a Matlab cluster analysis (k-means) are shown as triangles for comparison. (*B*) For the Fourier analysis, the projection of the labeled cells in (*A*) onto the regression line was transformed into a density histogram. Peaks and troughs in the histogram illustrate the density variation of labeled cells along the length of the regression line. Fourier analysis of this density profile gave a F1 component with a modulation of 1.79 mm. (*C*) The 2 histograms show the distributions of cluster spacing for parasagittal sections from one series through V5/MT. On the left, the results for cluster spacing estimated with the Fourier F1 component were plotted; on the right, the mean center distances of the clusters as determined from k-means analysis for the same sections were plotted. Dashed lines indicate mean cluster spacing for this V5/MT series, which was 2.07 mm for the Fourier analysis and 2.39 mm for the k-means analysis.

points in the neighboring clusters and ranges from +1 to –1, equivalent to a correlation coefficient). The results of the k-means analysis provided location of cluster centers. The analysis was done separately along layer 6 and layers 2–4 to avoid "kmeans" assigning a false cluster center in layer 5 because the distance between a cluster of labeled cells in layers 2–4 and one in layer 6 could be smaller than the distance between clusters along the layers. We calculated the mean vector distance from the sum of the shortest intercenter vector distances of the clusters, including the center of the injection site as a "cluster center."

*3. Vector Analysis and 2D Autocorrelation Analysis*

For the flatmounted material, we examined the distribution of labeled cells from the injection center in a one-in-two or one-in-three series of flatmounted sections. For radial vectors originating from the injection site at 30° sector angles, we calculated the vector distance to each labeled cell, analyzed this distribution in sectors, and fitted each of the distributions through running median averaging (Matlab "smooth" function with "Savitzky–Golay" filter) to determine the position of peaks. We also compared vector distances in the dorsoventral versus mediolateral axis of V5/MT. By aligning one series of sections from one animal according to fiducial landmarks, we could extend the data analysis to the whole series of flatmounted sections with CTb labeled cells. This gave us a depth profile of the pattern of label within V5/MT as a whole. In addition, we converted the distribution of labeled cells into a 2D density histogram (bin width 100 μm) and then examined this, for each flatmounted section in a one-in-two or one-in-three series and for the series as a whole, with a 2D autocorrelation function (Matlab, "xcorr2"). The normalized 2D autocorrelation power distribution was then analyzed sector-by-sector as for the vector method above, radially from the injection site at 30° angles. We calculated the vector distance to each value of the power, analyzed this distribution in sectors, and fitted each of the distributions through running median averaging (Matlab "smooth" function with Savitzky–Golay filter) to determine the position of peaks in the 2D autocorrelation power distribution. This provided another measure of the labeled cell distributions within a section and across the series of sections.

## Results

We investigated the pattern of intrinsic horizontal connections within cortical area V5/MT in 9 hemispheres from 7 animals. We pressure injected a small volume of CTb into superficial and/or deep layers of V5/MT (see Fig. 1*B*). Injection sites usually had a diameter of about 1 mm (including halo) and spanned several layers. We examined the distribution of retrogradely labeled cells within V5/MT in either 1) parasagittal sections through V5/MT, which show the pattern of label across the 6 layers along the long dorsoventral axis (4 hemispheres from 4 different animals) or 2) tangential sections of cortical flatmounts, which provide a view of the 2D pattern of label within a layer (5 hemispheres from 3 animals).

### *Intrinsic Connectivity in V5/MT—Examination of Parasagittal Sections*

The darkly stained CTb injection site with labeled fibers emanating from it was usually visible on 2–3 parasagittal sections of a one-in-five series through V5/MT (Figs 1*B* and 3*C*), which is equivalent to about 0.75 mm. The effective uptake zone for the retrograde tracer CTb is typically defined as the dark core where no cell bodies and fibers can be discerned (e.g., Jeffs et al. 2009), around this is a dense halo of labeled fibers. Injection site cores in this study had a mean diameter of 735 μm (Table 1). While we cannot exclude low-level diffusion of tracer outside the core area, this did not seem effective in labeling cells. For instance, in Figure 1*D*, any spread of tracer into layer 6 did not result in a significant number of stained cell bodies in this layer. Retrogradely labeled cell bodies were distributed throughout most of the dorsoventral extent of V5/MT along the layers. For an injection site placed centrally with respect to the dorsoventral extent of V5/MT, the dorsoventral spread of labeled cell bodies was typically 6 mm on either side (Figs 1*C* and 3*C*). In the axis orthogonal to the sections, the short mediolateral axis of V5/MT, labeled cells were found in sections up to 2 mm on either side of the sections carrying the tracer injection.

Estimates of area for V5/MT vary depending on a variety of factors: for instance, histological methods, species, weight of animals and whether V5/MT is considered to extend into the less densely myelinated area in the fundus of the STS. Using myeloarchitecture, V5/MT in *Macaca fascicularis* was estimated to extend 10 × 3.5 mm (Van Essen et al. 1981). Based on the striate projection to the STS, the dorsoventral axis of V5/MT in the rhesus macaque was estimated to be around 12 mm (Ungerleider and Mishkin 1979). The extent of label we saw

**Table 1**
Injection sites and cluster separation determined by Fourier and k-means analyses for parasagittal sections

| Hemisphere | Injection site core | | | Cluster separation—Fourier method | | Cluster separation—k-means method | |
|---|---|---|---|---|---|---|---|
| | RF center (*x*,*y*) | Layer | Dimension (μm) | Superficial layers (mm) | Layer 6 (mm) | Superficial layers (mm) | Layer 6 (mm) |
| M106L | ca. 17°,−15° | 1–6 | 667 × 750 | 2.21 ± 0.13 | 1.79 ± 0.14 | 1.67 ± 0.13 | 2.04 ± 0.13 |
| M114L | 3.7°,−1.2° | 5–6 | 888 × 500 | 2.15 ± 0.11 | 1.91 ± 0.12 | 1.92 ± 0.09 | 1.63 ± 0.11 |
| M115R | −13.7°,−10.7° | 2–3 | 909 × 750 | 2.07 ± 0.13 | — | 2.39 ± 0.15 | — |
| M118L | 21.3°, −14° | 2–4 | 667 × 750 | 2.35 ± 0.18 | 1.51 ($n$ = 1) | 2.01 ± 0.08 | 1.39 ($n$ = 1) |
| Average | | | | 2.17 ± 0.07 | 1.83 ± 0.09 | 2.10 ± 0.08 | 1.82 ± 0.09 |

Note: The RF location, layers, and dimensions of the core injection sites are provided. The RF center for M106L was an estimate based on a nearby recording; other RFs were recorded directly prior to injection. Mean cluster separations (mm) ±SEM are shown separately for superficial and deep layers and for each V5/MT as well as averaged across animals. Injections in M115R and M118L were placed in the superficial layers, which yielded few retrogradely labeled cells in layer 6. Average cluster spacing assessed by the 2 quantitative methods neither differed significantly for superficial layers (ANOVA, $P = 0.53$) nor did it differ between the 2 methods for layer 6 (ANOVA, $P = 0.90$). When we compared cluster spacing between superficial layers and lower layers (for M106L and M114L only), statistical results were not consistent (2 sample $t$-tests assuming unequal variances). For the Fourier analysis, in one case, there was no difference (M114L, $P = 0.16$) and in the other, there was (M106L, $P < 0.05$). Analyzing the same data with k-means, cluster spacing was not significantly different in either case ($P > 0.05$).

across parasagittal sections suggested that our injection sites retrogradely label cells throughout most of V5/MT. The lateral extent of connections to the injection site will be further quantified in the 2D flatmount data in the second part of the Results. For the parasagittal sections, we restricted our analysis to within the borders of the densely myelinated area identified with Gallyas.

The laminar distribution of labeled cells was distinct. Retrogradely labeled cells were found predominantly within layers 2 and 3 and for deep layer injection sites also in layer 6 (Fig. 3). The laminar pattern of labeled cells varied with location of the injection site. Only a few labeled cells were found in layer 6, following injections restricted to the upper layers (Fig. 1). A clear gap between CTb labeled cells in superficial and deep layers of V5/MT was visible due to very sparse label in layer 5 and at least the lower part of layer 4. This pattern was confirmed when we co-stained sections with SMI-32 (as well as for CTb) (Fig. 2), which, in V5/MT, labels pyramidal cells in layers 3 and 5.

The cortical layers that contained retrogradely labeled cell bodies varied with placement of the injection site in either superficial layers or layer 6. The distribution of CTb labeled cells across the different layers suggests that cells in the upper layers of V5/MT receive long-range lateral input predominantly from other upper layer cells because tracer injections with the effective uptake zone restricted to the upper layers (M115R and M118L) retrogradely labeled cell bodies only sparsely in layer 6 (Table 1). Thus, the nerve endings of V5/MT neurons that took up the tracer at the injection site came predominantly from cell bodies located in the upper layers. In contrast, a tracer injection restricted to the deep layers of V5/MT retrogradely labeled cell bodies in upper and deep layers (M114L; Fig. 3). This suggests that cells in the deep layers receive extensive horizontal input from superficial layers as well as layer 6.

Qualitative inspection of individual parasagittal sections showed that labeled cells were not uniformly distributed along the layers but were concentrated in distinct regions showing a high density of labeled cells. These regions appeared to form clusters within V5/MT (Figs 1*B–D*, 2A [black dots], and 3*A*,*C*). The clusters closest to the injection site were often easy to identify at low magnification, whereas those further away had fewer labeled cells and were only obvious under higher magnification. The closest cluster was typically 2 mm from the center of the injection site. Immediately around the injection site core, there was an area of fibers that was densely stained

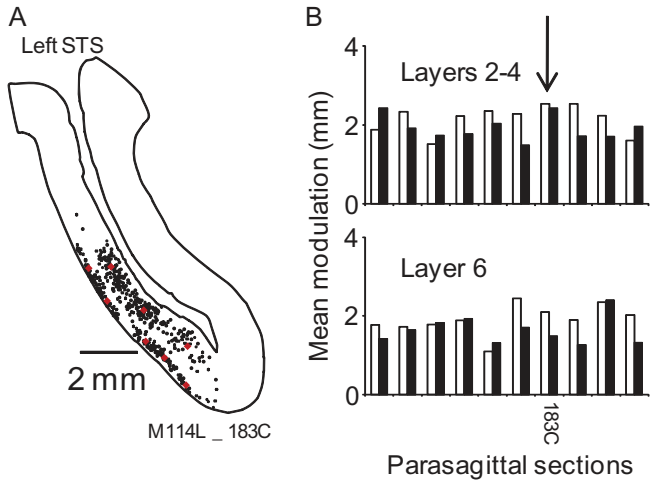


**Figure 5.** Comparison of Fourier- and k-means-based analysis of labeled cell clusters. (*A*) The distribution of labeled cells is shown for a single section. As derived from the k-means analysis, the locations of the cluster centers were superimposed as red diamonds for the superficial layers and layer 6. B. The mean cluster spacing derived from Fourier (open bars) and k-means cluster results (black bars) were compared for a one-in-five series of parasagittal sections through the mediolateral extent of V5/MT. Data were presented separately for superficial layers (upper histogram) and layer 6 (lower histogram). The results from the section 183C presented in (*A*) are indicated by the arrow. The 2 measures for distance between clusters of labeled cells showed good agreement.

and where cell bodies were difficult to discern. However, inspecting sections under high magnification, it was apparent that cortex beyond this zone but before the nearest cluster of labeled cells usually showed a few labeled cells, which were clearly discernible.

To quantify the pattern of connectivity across different sections and for different animals, using Neurolucida, we drew a one-in-five series of sections for each of 4 V5/MTs from 4 animals for which the cortex had been sectioned in the parasagittal plane. Borders of V5/MT were confirmed on each section using another one-in-five series of Gallyas-stained sections (Fig. 3*B*). We plotted the location of each CTb labeled cell within the outline of a parasagittal section around the STS, including the region around V5/MT. In the example in Figure 3, the injection site was located deep in layers 5 and 6. The majority of CTb labeled cells were found in superficial layers and deep layer 6. Again, the scarceness of labeled cells within layer 5 and at least part of layer 4 is clearly apparent in these

sections, as are regions of higher cell density, forming cell clusters (Fig. 3*C*).

To investigate whether the pattern of labeled cells followed a stereotypical periodicity, we compared labeled cell positions with 2 different quantitative analyses, namely Fourier and k-means analyses. In the case of Fourier analysis, we fitted best-fit polynomial lines to the distribution of labeled cells within superficial and deep layers separately (Fig. 4*A*) and then projected the labeled cells orthogonally onto this line to generate a density histogram of labeled cells along the dorsoventral length of V5/MT (Fig. 4*B*). The example histogram shows 5 peaks of high density of labeled cells, which identify clusters of labeled cells. We then determined the F1 component from Fourier analysis. The F1 component represents the primary modulation frequency for the distribution density of labeled cells. This provides a length measure of the mean repeat distance (1.79 mm in the pictured example) between high-density areas along the dorsoventral axis of V5/MT.

For the k-means cluster analysis, we first determined the number and center coordinates of clusters through minimizing the overall distance from cells to their nearest center using the untransformed 2D distribution of labeled cells as found within the parasagittal section (centers denoted by triangles in Fig. 4*A*). We then calculated the mean intercluster separation (2.05 mm in the pictured example). Figure 4*C* summarizes the distributions of intercluster spacing measured with Fourier and k-means analyses across a one-in-five series of sections from one V5/MT hemisphere. This V5/MT injection was restricted to the superficial layers and consequently only few cells were labeled in layer 6. Analysis of the superficial layer data showed the good agreement between the two measures (example in Fig. 4*C*: mean ± 1 standard error of mean [SEM], Fourier method: 2.07 ± 0.13 mm, and k-means method: 2.39 ± 0.15 mm; analysis of variance [ANOVA], $P = 0.08$). Figure 5 compared the two quantitative measures across another V5/MT case (the series depicted in Fig. 3*C*). In this V5/MT, the CTb injection site

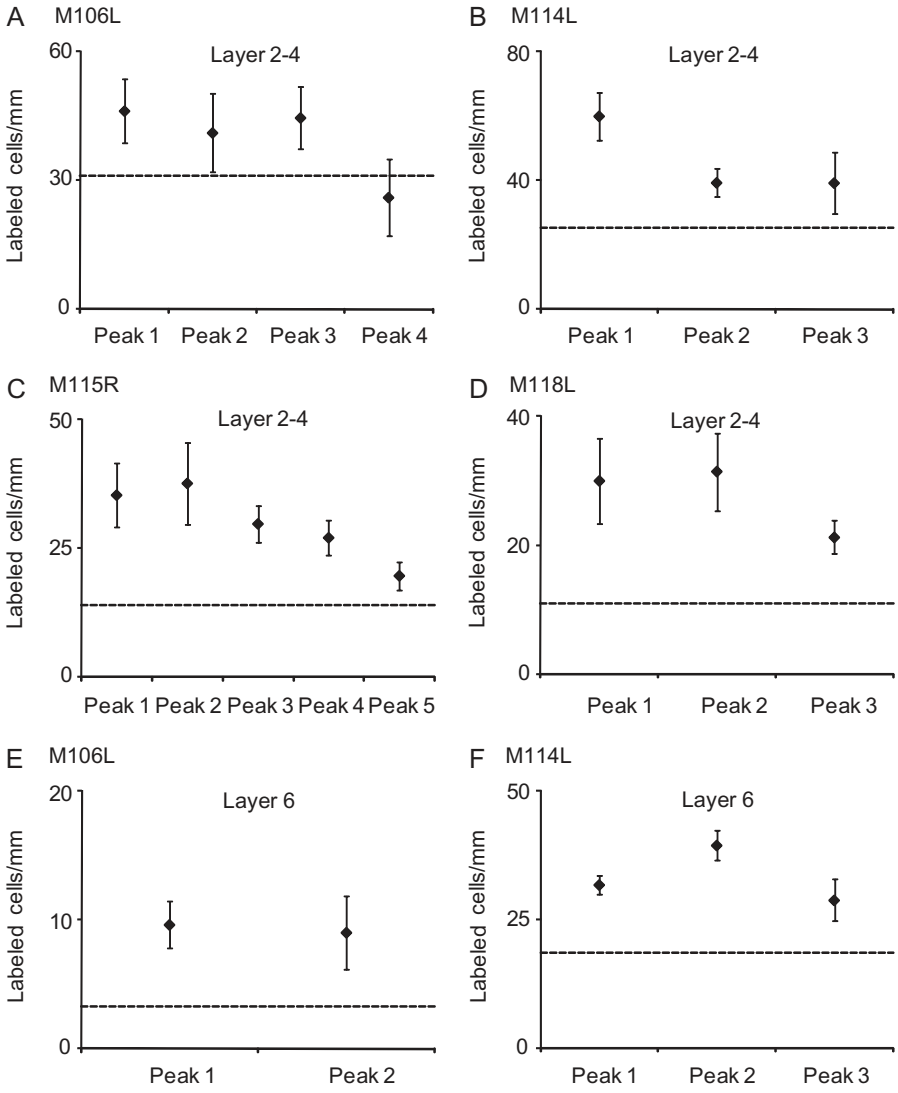


**Figure 6.** Peak and background density of labeled cells for parasagittal sections. Using the density profile for the Fourier analysis, the peak densities of clusters were plotted. Peak 1 was always the average of the first peak density on either side of the injection site in each section. The amplitude of the F0 component of the Fourier analysis provided an estimate of the density of background labeling and is shown as the dashed horizontal line. (*A*) Data from the superficial layers of hemisphere M106L. (*B*) Data from the superficial layers of hemisphere M114L. (*C*) Data from the superficial layers of hemisphere M115R. (*D*) Data from the superficial layers of hemisphere M118L. (*E*) Data from layer 6 of hemisphere M106L. (*F*) Data from layer 6 of hemisphere M114L. Error bars depict SEM.

was localized to layers 5 and 6 and extensively labeled cells in layer 6 and superficial layers. We plotted the results for the Fourier and k-means methods separately for superficial layers (Fig. 5*B*) and deep layers (Fig. 5*B*, layer 6). The mean cluster spacings obtained by the 2 methods (superficial layers: 2.17 and 2.10 mm and deep layers: 1.83 and 1.82 mm, respectively) were not significantly different from one another (ANOVA; superficial layers $P = 0.53$ and deep layers $P = 0.90$). Table 1 summarizes the mean values of intercluster separation for one series of sections through V5/MT for each hemisphere and the average across the 4 hemispheres. In the 2 parasagittal hemispheres, where the injection site core incorporated layer 6 (M106L and M114L), there was no systematic difference between superficial layers and layer 6 cluster distances. Our present data, therefore, provide no evidence to indicate that there is any consistent difference between superficial and deep layer cluster spacing.

To reveal the overall distribution of labeled cells, apart from the periodicity, we also estimated the background density of labeled cells and related this to the pattern of peak densities in the clusters. The background labeling was estimated from the amplitude of the F0 component of the Fourier analysis, the peak density in each cluster was taken as the maximum density in the density histogram used for the Fourier analysis. Within superficial layers, peak densities appear to decrease with distance from the injection site on top of a steady background of labeled cells of between 11 and 31 labeled cells per millimeter (Fig. 6*A–D*). The data for layer 6 showed a similar density of background label but no decrease in peak cluster density with distance from the injection site (Fig. 6*E–F*).

Thus, we found that a single injection of a retrograde tracer in V5/MT revealed wide-ranging horizontal connections along layers 2–4 and 6 of this extrastriate visual area. Those projections were clustered. Two independent analysis methods estimate that the average spacing between clusters was 2 mm along the dorsoventral axis of V5/MT. The peak density of labeled cells for each cluster decreased with distance from the injection site. In order to get a clearer picture of the distribution of neurons within the 2D layer that are connected to a single injection site, we further investigated V5/MT's intrinsic connectivity in cortical flatmounts.

### *Horizontal Connectivity within the Layer Sheet—Examining Flatmounted V5/MT*

Flatmounted cortical hemispheres were tangentially sectioned at 70 μm thickness. The dense region of CTb label of the injection site with its halo (diameter about 1 mm) was clearly visible in each flatmount. Tangential sectioning of the thin tissue sheet limited analysis to superficial cortex over a depth from about 280 μm to a maximum of 1600 μm from the pial surface comprising layers 2–5. In order to delineate V5/MT, we used the pattern of cytochrome oxidase (CO) label (Sincich et al. 2003) on sections from another series as well as the physical boundary of the fundus of the STS. The V5/MT axes for the flatmounts sheets were approximated to the intact brain. The putative dorsoventral axis was taken to be parallel with the upper part of the STS sulcus along the long axis of the CO label. Labeled cells were distributed throughout V5/MT and also just outside of its boundaries. We have limited our analyses to those labeled cells within and at the boundaries of V5/MT.

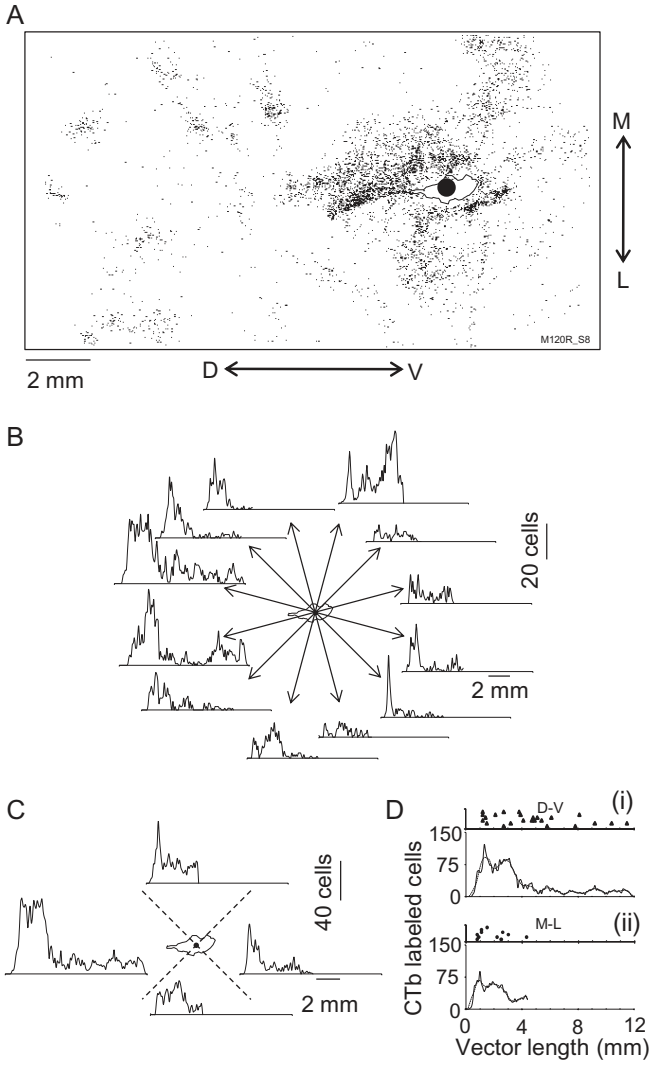


**Figure 7.** CTb labeled cells in a single flatmounted tangential section through V5/MT. (*A*) The CTb injection site was defined by the contour with the filled circle, located toward the right of the section. Each small black dot shows the position of one CTb labeled cell within V5/MT. (*B*) A vector length for each labeled cell was determined from the center of the injection site. Each of the twelve density profiles represents the distribution of vector lengths within a 30° sector highlighting the anisotropic distribution of labeled cells. (*C*) As in (*B*) but for 90° sectors based on a division into medial (top), ventral (right), lateral (bottom) and dorsal (left) regions centered on the injection site. D. Each of the 30° sector distributions in (*B*) was fitted (Matlab "smooth" function) and the peak values were determined from each of the twelve fitted functions. The vector distances from the injection site to the peaks in the distribution of cells from all 12 sectors were combined such as to generate density profiles for 2 V5/MT axes of interest: one representing the dorsal and the ventral, and the second the medial and the lateral. (i) Dorso-ventral (D-V) axis: The peaks in the density profile (upper part) represent the vector lengths from the injection site to the cluster center. The lower part illustrates the density distribution (continuous line) together with the fitted distribution (dashed line). (ii) Medio-lateral (M-L) axis: as in (i), distances of cluster centers (upper part) and the fitted density distribution (lower part).

In the first case (Fig. 7), we analyzed the distribution of label over an extent of approximately 16 mm in the longer dorsoventral axis of V5/MT and 9 mm in the shorter mediolateral axis. The position of each labeled cell in a tangential section through V5/MT was recorded with Neurolucida (Fig. 7*A*; depth 490–560 μm from pial surface). The labeled cells were not evenly scattered. Close to the injection site, we found

several dense bands of labeled cells. Further away from the injection site, the number of labeled cells declined sharply, but clusters with a higher density of labeled cells were visible.

We quantified the connectivity of V5/MT cells to the injection site through a radial density analysis. Since cells had to be retrogradely labeled from the injection site, this was the direction of the investigated intrinsic connections. Each cell was assigned a vector originating at the injection site; vector length gave the distance and its angle the position. When we summed the radial distribution of labeled cells in 30° sectors for the section in Figure 7, the resultant cell density histograms showed clear peaks, which delineated regions with higher densities of labeled cells (Fig. 7*B*). Summing the results in 90° sectors where each sector represented the dorsal, medial, ventral, and lateral regions of V5/MT illustrates—similarly to the parasagittal sections—that on top of a low background density of labeled cells, there were clear high-density peaks of labeled cells. The density of labeled cells in these clusters declined with distance from the injection site. The analysis in 90° sectors also underlines the anisotropic distribution of labeled cells in the dorsoventral axis and mediolateral axis (Fig. 7*C*). The data were also asymmetric along each axis: for this section, asymmetry of the number of labeled cells in the dorsoventral axis was by a factor of 4.2, when either side of the injection site was compared. In the mediolateral axis, the factor was 2.0.

To determine the centers of the high-density regions (the cluster centers), we fitted a distribution (Matlab "smooth" function) and then determined the peak values for each of the 12 sectors. Then, we assessed peak distances from the injection site by combining the results from these sectors into 2 axes, the dorsal with the ventral and the medial with the lateral, to determine the variation in density along these 2 axes (Fig. 7*D*). In the dorsoventral axis of V5/MT, the density profile and its fitted distribution showed clusters of labeled cells almost 12 mm away from the injection site (Fig. 7*Di*). Plotted above the density plot, cluster centers were particularly concentrated at 1.5 and 5 mm from the injection site. Over the longer range, more distinct clusters of labeled cells could be identified. For this flatmounted section (M120R_S8), the mean distance from the injection site to the nearest cluster center in the dorsoventral axis was 1.53 mm (SEM ±0.24). For the mediolateral axis (Fig. 7*Dii*), most labeled cells were found within 5 mm of the injection site, with the nearest cluster centers at 1.03 mm (SEM ±0.11) from the injection site. Examining all cluster centers for this section, the average radial separation between clusters was 2.07 mm (SEM ±0.29) in the dorsoventral axis of V5/MT and 1.36 mm (SEM ±0.15) in the mediolateral axis, which was the smallest average cluster spacing we measured.

In another example section through layers 2/3 (depth 560–630 μm) from the right V5/MT of a different animal (Fig. 8*A*), the radial density distributions of labeled cells together with the fitted functions had distinct peaks at distances of about 1.5 and 3 mm and 4.5–5 mm away from the injection site (Fig. 8*B*), in both the dorsoventral (in red) and the mediolateral (in blue) axes. For this section, the nearest cluster centers to the injection site were in the dorsoventral axis at 1.6 mm (SEM ±0.17) and in the mediolateral axis 1.52 mm (SEM ±0.04). After examining all clusters for this section, we estimated the average cluster separations: dorsoventral 1.83 mm (SEM ±0.13) and mediolateral 1.71 mm (SEM ±0.15).

We analyzed cluster size and separation for 5 hemispheres, using a one-in-three series or better. The average number of clusters per section was 24, with a mean cluster size of 521 μm (at half of peak height). Because the distribution of cluster size was asymmetric, we also calculated a mode of 300 μm after

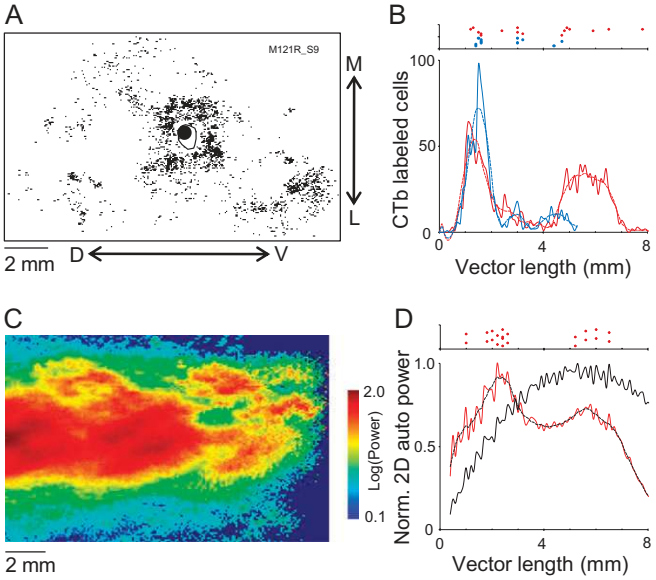


**Figure 8.** Analysis of CTb labeled cells in a single flatmounted section. (*A*) A Neurolucida drawing of a flat-mounted section through V5/MT. The injection site (shown as a contour in black with filled circle) was surrounded by clusters of CTb labeled cells (black dots). (*B*) The lower part shows the density distributions for the cells in this section and its fitted "smooth" function (Matlab; dashed line). The red lines represent the data from the dorso-ventral axis, the blue lines the data from the medio-lateral axis. The vector location of the cluster centers were plotted above, for the dorso-ventral axis (filled red diamonds) and for the medio-lateral axis (filled blue dots). (*C*) A colour rendered profile was derived from the 2-dimensional autocorrelation analysis of the distribution of labeled cells in (*A*). The dark red areas represent areas of label where the autocorrelation analysis indicated peaks. D. The vector lengths to peaks in the autocorrelation power function were determined for radial sectors (30° angles) and are plotted as red diamonds (upper part). The normalized autocorrelation power values were plotted against vector lengths below. The red continuous line is the sum of the power values according to vector distance for data from (*C*) (dashed black line is the best fit to these data). The continuous black line is the sum of the power values for an array of points at an equivalent density but randomly located within the dimensions defined by the area of V5/MT analysed in (*A*). The autocorrelation analysis underlines that the distribution of labeled cells through V5/MT was not random.

**Table 2**
Cluster spacing determined by vector distance analysis for flatmounted sections

| Animal code | Vector method; Radial peak separation (mm) | | | |
|---|---|---|---|---|
| | First cluster—DV axis | Average spacing—DV axis | First cluster—ML axis | Average spacing–ML axis |
| M120L | 3.05 ± 0.25 | 2.64 ± 0.20 | 1.92 ± 0.10 | 2.14 ± 0.12 |
| M120R | 1.99 ± 0.16 | 2.17 ± 0.13 | 1.53 ± 0.13 | 2.01 ± 0.10 |
| M121L | 2.48 ± 0.22 | 2.32 ± 0.14 | 2.3 ± 0.19 | 2.18 ± 0.16 |
| M121R | 1.65 ± 0.11 | 1.98 ± 0.09 | 1.68 ± 0.15 | 1.83 ± 0.11 |
| M122L | 2.08 ± 0.15 | 2.3 ± 0.23 | 2.45 ± 0.23 | 2.8 ± 0.29 |
| Average | 2.24 ± 0.09* | 2.27 ± 0.07 | 1.95 ± 0.08* | 2.17 ± 0.07 |

Note: Results for one-in-three series of sections or better for each hemisphere are given in mean (mm) ± SEM. "First cluster" denotes the nearest cluster to the injection site and "Average spacing" denotes the average distance between clusters along lines originating from the injection site. The distance from injection site to first cluster differs significantly between the long and the short axis of V5/MT (ANOVA, $P < 0.02$*); DV, dorsoventral; ML, mediolateral.

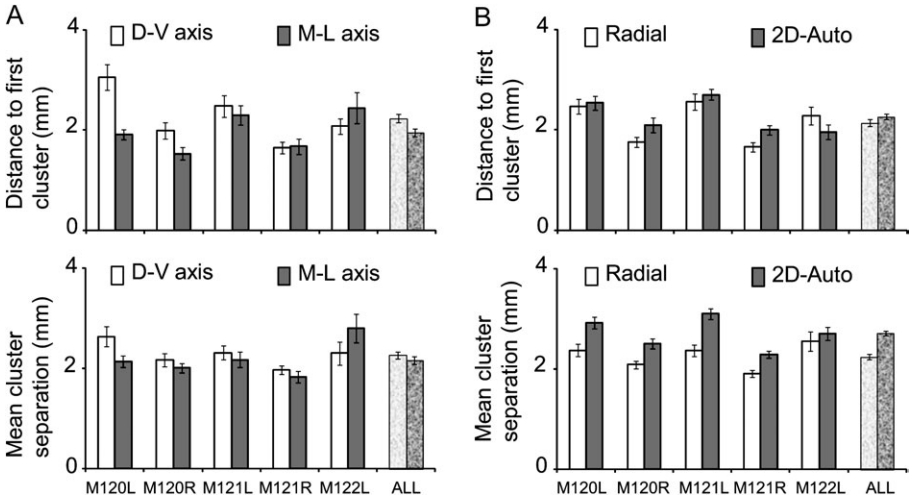


**Figure 9.** Quantitative analysis of the distribution of CTb labeled cells from flatmounted hemispheres. (*A*) Radial vector data were separated for the dorso-ventral (white bars) and medio-lateral axes (dark bars) of V5/MT. The upper histogram shows the mean distance from the injection site to the nearest cluster across the 5 analyzed hemispheres. The lower histogram plots averaged values for inter-cluster separations for V5/MT. The textured bars on the right side in both histograms represent the mean values. (*B*) The same radial vector data but plotted without separating the 2 axes (Radial; white bars) were compared with measures from 2D autocorrelation analyses (2D-Auto; dark bars). The upper histogram shows again the distance of the initial cluster from the injection site center and the lower histogram plots averaged values for inter-cluster separations for V5/MT. Error bars depict SEM.

**Table 3**
Summary of injection site dimensions, multiunit RF at each injection site, and the length of horizontal connections in the flatmounts

| Hemisphere | Injection site core | | RF eccentricity | RF size | Furthest cluster DV, mean (mm) ± SD | Furthest cluster ML, mean (mm) ± SD |
|---|---|---|---|---|---|---|
| | Layers (spread) | Dimensions (μm) | | | | |
| M120L | 3/4 (3–5) | 525 × 313 | 23° | 7° × 7° | 9.1 ± 2.3 | 9.7 ± 1.0 |
| M120R | 3 (3) | 1188 × 450 | 15° | 8° × 12° | 10.3 ± 1.8 | 7.5 ± 1.9 |
| M121L | 3 (3–4) | 1063 × 400 | 15° | 10 × 21° | 9.3 ± 1.6 | 6.9 ± 1.8 |
| M121R | 3 (3–5) | 1188 × 812 | 11° | 11° × 9° | 7.4 ± 1.1 | 6.2 ± 0.8 |
| M122L | 3 (2–3) | 412 × 250 | 39° | 21° × 26° | 8.2 ± 1.0 | 6.8 ± 2.7 |

Note: RF eccentricity and RF size were mapped qualitatively through multiunit recording just before the placement of injections. To estimate the range of the horizontal connectivity, for each section, we identified the furthest cluster of labeled cells (defined by vector analysis). For each hemisphere, we calculated the means and SDs across the same series of sections as analyzed in Table 2. SD, standard deviation; DV, dorsoventral; ML, mediolateral.

**Table 4**
Comparison of cluster spacing obtained by the radial vector distance and 2D autocorrelation analyses

| Animal code | Vector method | | 2D autocorrelation method | |
|---|---|---|---|---|
| | First cluster (mm) | Average spacing (mm) | First cluster (mm) | Average spacing (mm) |
| M120L | 2.47 ± 0.15 | 2.38 ± 0.12 | 2.54 ± 0.14 | 2.93 ± 0.12 |
| M120R | 1.76 ± 0.1 | 2.09 ± 0.08 | 2.1 ± 0.14 | 2.52 ± 0.1 |
| M121L | 2.57 ± 0.16 | 2.38 ± 0.11 | 2.71 ± 0.11 | 3.11 ± 0.11 |
| M121R | 1.67 ± 0.09 | 1.91 ± 0.07 | 2.0 ± 0.09 | 2.29 ± 0.07 |
| M122L | 2.28 ± 0.17 | 2.55 ± 0.19 | 1.97 ± 0.15 | 2.71 ± 0.13 |
| Average | 2.15 ± 0.06 | 2.25 ± 0.05** | 2.27 ± 0.06 | 2.72 ± 0.05** |

Note: The distances of the closest cluster of labeled cells to the injection site (First cluster) and the average cluster spacing are shown for each of 5 V5/MTs from 3 animals in millimeter (±SEM). The average spacing between clusters but not the distance to the cluster closest to the injection site differed significantly for the 2 methods (ANOVA, $P < 0.01$**).

discretizing the data. Generally, the cluster spacing obtained with the vector method tended to be comparable in the 2 axes of V5/MT and across hemispheres (Table 2 and Fig. 9*A*). The vector method, applied to all 5 hemispheres, gave an estimate of the cluster separation as 2.25 mm (see Table 4). This value was consistent with the cluster spacing derived from the Fourier method for parasagittal sections of 2.16 mm (Table 1). However, we found that in the mediolateral axis of V5/MT, the nearest cluster of labeled cells tended to be, at 1.95 mm, closer to the injection site than in the dorsoventral direction at 2.24 mm (ANOVA, $P < 0.02$) (Table 2). But the average radial cluster spacing across V5/MT flatmounts was not significantly different between the two axes (ANOVA, $P = 0.33$).

Using the same data, we also assessed for each hemisphere the distance of the furthest cluster from the injection site (Table 3). The maximum length of connections is anisotropic, with clusters labeled often further away in the dorsoventral (mean distance from injection site 8.9 mm) than the mediolateral axis (mean distance 7.4 mm). This gives an average anisotropy of 1.2. However, this was considerably more marked in some hemispheres, particularly in the sections with the strongest label. Along each axis, there can also be considerable asymmetry in the number of labeled cells on either side of the injections site (e.g., Fig. 6*C*). Across all 5 hemispheres, within the dorsoventral axis, the average number of labeled cells differed by a factor of 2.71 (SEM ±0.29) and within the mediolateral axis by a factor of 1.21 (SEM ±0.16). Some of the injection sites were placed close to the borders of V5/MT; this might contribute to the asymmetry of horizontal connections for a given axis (see, e.g., M120R in Fig. 7).

In order to confirm the quantitative measures of cluster spacing, we also analyzed cluster spacing with a 2D

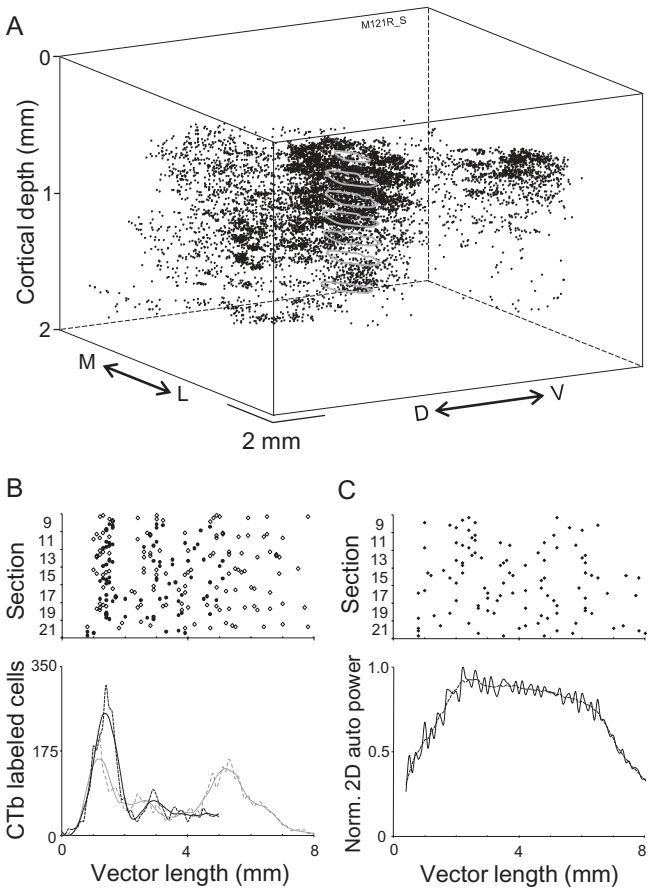


**Figure 10.** Quantitative analysis of CTb labeled cells for a one-in-two series of tangential sections through one flatmounted V5/MT. The series of tangential sections from a flatmounted hemisphere was taken from the same animal as Figure 7. (*A*) Individual sections were aligned using the center of the injection site as a guide. The CTb injection site was outlined as gray contours. CTb labeled cells (black dots) are shown at their cortical depth in a 3-dimensional view. Some clusters of labeled cells were discernible running orthogonal through the tangential sections. (*B*) The upper figure shows the vector location of the cluster centers in the dorso-ventral axis (open diamonds) and for the medio-lateral axis (filled dots), separately for each flatmount section. The density distribution (lower figure) is the combined distributions of all these sections but separated into the dorso-ventral (pale dashed line) and medio-lateral axes (black broken line). The solid lines in each case are the fitted functions to the data, from which the cluster centers were derived. Although labeled cells were widely distributed, for both axes, labeled cells were clearly concentrated at 1.5-2 mm and at 3 mm. In the dorso-ventral axis, the distribution of labeled cells also peaked between 5 and 6 mm. (*C*) The upper figure shows the vector lengths to peaks in the 2D autocorrelation power function plotted for each flatmounted section. The combined 2D autocorrelation power distribution (normalized) for all flatmounted sections is shown below (lower figure, solid line). The dashed line is the fitted function to these data.

autocorrelation analysis (see example in Fig. 8*C*). We estimated the distance of centers of labeled cell clusters from the injection site by measuring the change in the autocorrelation power (Fig. 8*D*, red). Derived from the 2D autocorrelation analysis, for the section in Figure 8, the value for the nearest cluster center to the injection site was 1.97 mm (SEM ±0.15) and the average separation between clusters of labeled cells was 2.53 mm (SEM ±0.19) (see Supplementary Material for a further example section from another hemisphere).

Across all 5 hemispheres, the 2 methods for quantification resulted in small differences in average cluster spacing but none in the distance estimates to the first cluster (Fig. 9*B* and Table 4). The autocorrelation method resulted in a larger estimate of average cluster spacing. None of these differences was related to the placement of the injection site (data not shown).

For each hemisphere, we also aligned an entire series of tangential sections through V5/MT to visualize the 3D distribution of labeled cells through the depth of cortex. Figure 10*A* shows a one-in-two series through one hemisphere ($n$ = 7 sections) (see Supplementary Material for another example for V5/MT). The most superficial tangential section we could analyze was 280 μm below the pial surface and the deepest was at 1470 μm. Within V5/MT, a single CTb injection retrogradely labeled cells across a wide area; denser patches of labeled cells were apparent, some of which appeared to form a vertical column across sections. The pattern of labeled cells across the tangential sections was consistent with that found in parasagittal sections. The combined density distribution across tangential sections had distinct peaks along the dorsoventral axis (dashed line, lower Fig. 10*B*) and along the mediolateral axis (broken line, lower Fig. 10*B*) indicating consistent spacing of clusters across sections. For this V5/MT, the center of the nearest cluster was on average 1.65 mm from the injection site in the dorsomedial axis and 1.68 mm in the mediolateral axis (Table 2). The average radial separations between cluster centers were, respectively, 1.98 and 1.83 mm. The equivalent measures derived from the 2D autocorrelation analysis were slightly higher but comparable. The nearest cluster centers to the injection site were at about 2.0 mm and the average radial separation between clusters was 2.29 mm (Fig. 10*C* and Table 4).

In summary, the retrograde tracer CTb placed in small injections into V5/MT was taken up by nerve terminals, transported along a wide-ranging network of horizontal connections and labeled identifiable clusters of cell bodies up to 10 mm away. The clusters of labeled cells closest to the injections site were at about 2 mm. Two separate quantitative measures identified the average spacing between labeled clusters at just over 2 mm, with a slightly larger estimate of cluster spacing for the autocorrelation method. But estimates of cluster spacing were generally consistent section-by-section and between hemispheres.

## Discussion

We examined the local intracortical circuitry of V5/MT with injections of the retrograde tracer CTb. A small injection site labeled cell bodies over a long range throughout most of the extent of V5/MT. In parasagittal sections, the pattern of connectivity in different layers was related to the location of the injection site: deep layer injections heavily back-labeled cells in layers 2–3 and 6 and upper layer injections labeled cells in layers 2–3 and sparsely in layer 6. For all injection site locations, we found very few CTb labeled cells within layer 5 and at least the lower part of layer 4. The pattern of labeled cells within superficial layers and layer 6 was not uniform but clustered. The results point to a pattern of local connections within V5/MT by means of which clusters of cells at an average spacing of approximately 2 mm are preferentially connected.

### *Comparison of Range of V5/MT Horizontal Connectivity to Intrinsic Connectivity in Other Cortical Areas*

In the rhesus macaque, we found retrogradely labeled cells that, in the dorsoventral axis, were as far as 8–10 mm away from

the injection site. While clustering of horizontal connectivity has been shown in primary visual cortex (V1) of the same species, clusters were generally found much closer to the injection site, up to 4.5 mm away (Rockland and Lund 1983; Lund et al. 2003). However, axons of individual Meynert cells, which are located in layer 6 of V1 and also send projections to V5/MT, can extend up to 8 mm within V1 (Rockland and Knutson 2001; Li et al. 2003). While this is comparable to the longest intrinsic connections in our study, if these numbers are scaled by the total size of the 2 cortical areas, 8 mm in V1 would still appear to be closer than 8 mm in V5/MT. It has been estimated that the extent of horizontal connectivity in V1 corresponds to the neuronal low contrast summation field of neurons' RF (Angelucci, Levitt, Walton, et al. 2002). The intercluster repeat pattern in V1 was, at a separation of approximately 500 μm, much shorter than that in V5/MT. Do these differences in horizontal connectivity between V1 and V5/MT in the rhesus macaque simply reflect the different scales of cortical representations or do they reflect differences in functional architecture?

The cortical magnification factor in V5/MT is up to 5 times smaller than in V1 (Albright and Desimone 1987), which suggests that horizontal connectivity covers a larger part of the visual field in V5/MT. At 10° eccentricity, V5/MT magnification factor levels off at 0.2 mm per degree. For the injection site shown in Figure 7, with a pictured horizontal range of about 10 mm, this would correspond to a coverage of about 50° of the visual field. Based on the known distribution of RF sizes in V5/MT, we probably underestimated the minimum response field. While RFs in V5/MT are considerably larger than in V1, there is also a large degree of RF overlap, even when an electrode is moved through several millimeters of cortex. Moreover, maps can be distorted (Desimone and Ungerleider 1986). Whichever way one chooses to argue these points, the range of inputs suggested by our anatomical data is considerably larger than the minimum response field we measured at the injection site.

A further issue is that many V5/MT neurons have large antagonistic surrounds. Although the size of the surrounds varies with the different methods of estimation, they can be 3–4 times the classical RF or larger (Tanaka et al. 1986; Raiguel et al. 1995). Inhibitory surrounds are often anisotropic and can also be one-sided asymmetric, few are concentric (Xiao et al. 1997). While this would potentially fit well with the pattern of label we found in the flatmounted sections, we do not have data about the inhibitory surrounds of neurons at the injection site. Thus, a direct relationship cannot be established. The size of antagonistic surrounds has also been found to vary with cortical layer (Raiguel et al. 1995). Again, it fits well with our data on horizontal connectivity that these surrounds are largest in layer 2. However, the large surround sizes for layer 5 cells could only be explained by inputs from other layers, and indeed, we found in parasagittal sections that lower layer 5/6 injections retrogradely labeled cells extensively in the upper layers, again in a clustered fashion (see Fig. 3).

Increasing lengths of intrinsic connections have been found as one ascends the visual cortical hierarchy. A comparative study of horizontal connectivity in areas V1, V2, V4, and 7a of the rhesus macaque found increasing spread of horizontal connectivity and increasing interpatch distance (Amir et al. 1993). In both these parameters, the results from area 7a were comparable to the results presented in this paper. Similarly, results of horizontal connectivity in inferotemporal cortex also showed connections of up to 8 mm and larger intercluster separation than in V1 (Tanigawa et al. 2005). More generally, evidence suggests that the distance between cortical clusters and cluster size scale in a species-independent way and in the primate, that both increase from occipital cortex to prefrontal cortex (Douglas and Martin 2004; da Costa and Martin 2010)

### *Pattern of V5/MT Intrinsic Connectivity in Other Primates*

To our knowledge, intrinsic connections in MT have been studied systematically only in New World monkeys (Weller et al. 1984; Malach et al. 1997) (but see also Maunsell and Van Essen 1983c). In the owl monkey, horizontal connectivity in MT has been shown to be clustered. However, while here we found a reproducible pattern of connections in the rhesus macaque, the specificity of the horizontal connectivity in the owl monkey has been found to vary between individual animals (Malach et al. 1997). Furthermore, when anterogradely labeled axonal arbors were traced after biocytin injections in the owl monkey, the furthest axonal patches were found on average only 1.8 mm away from the injection site. However, survival times in that study were 8–12 h, whereas ours were 48–72 h; tracing axons is often more difficult than identifying filled cell bodies and CTb is considered to be a more sensitive tracer than biocytin.

The functional organization of MT of owl monkey also differs from V5/MT in the rhesus macaque. While there is evidence for columns of opposite direction preference in the owl monkey (Malonek et al. 1994), this primate species has also a complex compartmental architecture, whereby neurons sensitive to global and local motion are segregated into bands (Born and Tootell 1992; Malonek et al. 1994). In the rhesus macaque, this type of organization seems less pronounced (Tanaka et al. 1986; Komatsu and Wurtz 1988; Raiguel et al. 1995; Born et al. 2000). Unlike V5/MT in the rhesus monkey, there is little selectivity for binocular disparity in the owl monkey (Zeki 1980; Felleman and Kaas 1984). Based on the available functional data, it is not clear whether we should expect to find the same patterning of connections in the two primate species.

### *Functional Significance of the Clustered Pattern of Horizontal Connections in V5/MT of the Rhesus Macaque*

Anatomical columns in V1 and their connections have been shown to be functional units (Lund et al. 2003). There are no data directly linking connectivity and neurophysiology in V5/MT of the rhesus monkey, but there are data showing functional interactions and functional compartments within V5/MT. While our data can be accounted for in terms of the size of antagonistic surrounds in V5/MT, our results might seem to be at odds with some inferences about the nature of cortical architecture in V5/MT acquired from recording studies in the awake, behaving macaque. Based on interneuronal spike train cross-correlation, de Oliveira et al. (1997) suggested that the probability of coupling between V5/MT neurons dramatically decreased with cortical distance, so that little functional coupling could be found for neurons separated by more than 300 μm. However, electrode separations were not systematically sampled in this study and it was not clear whether the

pairs of neuronal recording sites were in the same layer. Our anatomical data suggest that it might be difficult to isolate strongly connected pairs of neurons unless the pairs of recording sites are both in layers 2–3 or in layer 6 and with a mean separation of 2 mm or possibly a multiple thereof. If the connectivity provides the basis of the antagonistic surround, many long-range connections should connect to inhibitory cells. Future studies should also assess the fraction of labeled cells in a given cortical volume. In order to estimate functional connectivity from anatomical data, these issues need to be considered.

In V5/MT of the rhesus monkey, 2 independent functional organizations have been identified. Based on neurophysiological recordings, V5/MT has been proposed to have a columnar organization for direction of motion such that a single 360° cycle of motion direction has been estimated to have a width of 800–1000 μm (Albright et al. 1984). Additionally, V5/MT has also a clustered organization for binocular disparity: Clusters of near- and far-tuned neurons are interspersed with neurons poorly tuned for disparity, each forming on average 300- to 700-μm-wide clusters (DeAngelis and Newsome 1999). The anatomical cluster repeat pattern of about 2 mm that we found approximates to 2 full cycles of the columnar organization for direction of motion. Our anatomical data are consistent with a functional organization where neurons with the same preference for direction of motion and with selectivity for binocular disparity are more strongly connected, but not exclusively so. This would fit with models of neuronal function and horizontal connectivity for the perception of structure-from-motion (Nawrot and Blake 1991; Bradley et al. 1998) and perceptual coupling of such stimuli (Grossmann and Dobbins 2003; Klink et al. 2009). Again, why particularly neurons in layer 5 would lack long-range horizontal projections within V5/MT is not clear, although it has been suggested that neurons in layer 5 are less direction selective than cells in other layers (Raiguel et al. 1995).

In conclusion, small injections of the retrograde tracer CTb have provided a detailed insight into the local circuitry of V5/MT. Long-range connections of up to 8–10 mm indicate that, as previously suggested, connections intrinsic to V5/MT can potentially support the antagonistic surrounds of V5/MT cells. The spacing of labeled cell clusters at approximately 2 mm suggests that this arrangement of connectivity may relate to the functional relationship between direction of motion columns and stereo depth columns.

## Supplementary Material

Supplementary material can be found at: http://www.cercor.oxfordjournals.org/

## Funding

BBSRC Project Grant (BB/C504943 to K.K.); Wellcome Trust Programme grant (065511/Z/01/Z to Andrew Parker). K.K. is a Royal Society University Research Fellow. W.B. is a Wellcome Trust Senior Research Fellow.

## Notes

The authors would like to thank Prof. Andrew Parker for critical advice and support throughout this project. We would like to thank Dr. Wei Wang for his invaluable expertise in building the pipette/electrode hybrid. We thank Dr Pamela Baker for her expert assistance with experimental procedures, and Ms Kathy Murphy, Dr Caroline Bergmann, and Mr John Cranley for invaluable veterinary support. *Conflict of Interest*: None declared.

## References

Albright TD. 1984. Direction and orientation selectivity of neurons in visual area MT of the Macaque. J Neurophysiol. 52:1106–1130.

Albright TD, Desimone R. 1987. Local precision of visuotopic organization in the middle temporal area (MT) of the macaque. Exp Brain Res. 65:582–592.

Albright TD, Desimone R, Gross CG. 1984. Columnar organization of directionally selective cells in visual area MT of the macaque. J Neurophysiol. 51:16–31.

Amir Y, Harel M, Malach R. 1993. Cortical hierarchy reflected in the organization of intrinsic connections in macaque monkey visual cortex. J Comp Neurol. 334:19–46.

Angelucci A, Levitt JB, Lund JS. 2002. Anatomical origins of the classical receptive field and modulatory surround field of single neurons in macaque visual cortical area V1. Prog Brain Res. 136:373–388.

Angelucci A, Levitt JB, Walton EJ, Hupe JM, Bullier J, Lund JS. 2002. Circuits for local and global signal integration in primary visual cortex. J Neurosci. 22:8633–8646.

Born RT, Groh JM, Zhao R, Lukasewycz SJ. 2000. Segregation of object and background motion in visual area MT: effects of microstimulation on eye movements. Neuron. 26:725–734.

Born RT, Tootell RBH. 1992. Segregation of global and local motion processing in primate middle temporal visual area. Nature. 357:497–499.

Bosking WH, Zhang Y, Schofield B, Fitzpatrick D. 1997. Orientation selectivity and the arrangement of horizontal connections in tree shrew striate cortex. J Neurosci. 17:2112–2127.

Bradley DC, Chang GC, Andersen RA. 1998. Encoding of three-dimensional structure-from-motion by primate area MT neurons. Nature. 392:714–717.

Cheng K, Hasegawa T, Saleem KS, Tanaka K. 1994. Comparison of neuronal selectivity for stimulus speed, length, and contrast in the prestriate visual cortical areas V4 and MT of the macaque monkey. J Neurophysiol. 71:2269–2280.

da Costa NM, Martin KA. 2010. Whose cortical column would that be? Front Neuroanat. 4:16.

de Oliveira SC, Thiele A, Hoffmann KP. 1997. Synchronization of neuronal activity during stimulus expectation in a direction discrimination task. J Neurosci. 17:9248–9260.

DeAngelis GC, Cumming BG, Newsome WT. 1998. Cortical area MT and the perception of stereoscopic depth. Nature. 394:677–680.

DeAngelis GC, Newsome WT. 1999. Organization of disparity-selective neurons in macaque area MT. J Neurosci. 19:1398–1415.

Desimone R, Ungerleider LG. 1986. Multiple visual areas in the caudal superior temporal sulcus of the macaque. J Comp Neurol. 248:164–189.

Douglas RJ, Martin KA. 2004. Neuronal circuits of the neocortex. Annu Rev Neurosci. 27:419–451.

Dubner R, Zeki SM. 1971. Response properties and receptive fields of cells in an anatomically defined region of the superior temporal sulcus in the monkey. Brain Res. 35:528–532.

Felleman DJ, Kaas JH. 1984. Receptive-field properties of neurons in middle temporal visual area (MT) of owl monkeys. J Neurophysiol. 52:488–513.

Gallyas F. 1979. Silver staining of myelin by means of physical development. Neurol Res. 1:203–209.

Geesaman BJ, Born RT, Andersen RA, Tootell RBH. 1997. Maps of complex motion selectivity in the superior temporal cortex of the alert Macaque monkey: a double-label 2-deoxyglucose study. Cereb Cor. 7:749–757.

Gilbert CD, Wiesel TN. 1989. Columnar specificity of intrinsic horizontal and corticocortical connections in cat visual cortex. J Neurosci. 9:2432–2442.

Grossmann JK, Dobbins AC. 2003. Differential ambiguity reduces grouping of metastable objects. Vision Res. 43:359–369.

Jeffs J, Ichida JM, Federer F, Angelucci A. 2009. Anatomical evidence for classical and extra-classical receptive field completion across the

discontinuous horizontal meridian representation of primate area V2. Cereb Cor. 19:963–981.
Klink PC, Noest AJ, Holten V, van den Berg AV, van Wezel RJA. 2009. Occlusion-related lateral connections stabilize kinetic depth stimuli through perceptual coupling. J Vision. 9:20, 1–20.
Komatsu H, Wurtz RH. 1988. Relation of cortical areas MT and MST to pursuit eye movements. III. Interaction with full-field visual stimulation. J Neurophysiol. 60:621–644.
Krug K, Cumming BG, Parker AJ. 2004. Comparing perceptual signals of single V5/MT neurons in two binocular depth tasks. J Neurophysiol. 92:1586–1596.
Li H, Fukuda M, Tanifuji M, Rockland KS. 2003. Intrinsic collaterals of layer 6 Meynert cells and functional columns in primate V1. Neurosci. 120:1061–1069.
Lund JS, Angelucci A, Bressloff PC. 2003. Anatomical substrates for functional columns in Macaque monkey primary visual cortex. Cereb Cor. 13:15–24.
Malach R, Schirman TD, Harel M, Tootell RB, Malonek D. 1997. Organization of intrinsic connections in owl monkey area MT. Cereb Cor. 7:386–393.
Malonek D, Tootell RB, Grinvald A. 1994. Optical imaging reveals the functional architecture of neurons processing shape and motion in owl monkey area MT. Proc R Soc Lond B Biol Sci. 258:109–119.
Marcar VL, Cowey A. 1992. The effect of removing superior temporal cortical motion areas in the macaque monkey: II. Motion discrimination using random dot displays. Eur J Neurosci. 4: 1228–1238.
Maunsell JHR, Van Essen DC. 1983a. Functional properties of neurons in middle temporal visual area of the macaque monkey. II. Binocular interactions and sensitivity to binocular disparity. J Neurophysiol. 49:1148–1167.
Maunsell JHR, Van Essen DC. 1983b. Single unit responses in the middle temporal area of the macaque: I. Direction, speed, and orientation. J Neurophysiol. 49:1127–1147.
Maunsell JHR, Van Essen DC. 1983c. The connections of the middle temporal visual area (MT) and their relationship to a cortical hierarchy in the macaque monkey. J Neurosci. 3:2563–2586.
Movshon JA, Adelson EH, Gizzi MS, Newsome WT. 1983. The analysis of moving visual patterns. In: Chagas C, Gattass R, Gross CG, editors. Study group on pattern recognition mechanisms. Vatican City: Pontifica Academia Scientiarum. p. 116–151.
Nawrot M, Blake R. 1991. A neural network model of kinetic depth. Vis Neurosci. 6:219–227.
Newsome WT, Britten KH, Movshon JA. 1989. Neuronal correlates of a perceptual decision. Nature. 341:52–54.
Newsome WT, Pare EB. 1988. A selective impairment of motion perception following lesions of the middle temporal visual area (MT). J Neurosci. 8:2201–2211.
Raiguel S, Van Hulle MM, Xiao DK, Marcar VL, Orban GA. 1995. Shape and spatial distribution of receptive fields and antagonistic motion surrounds in the middle temporal area (V5) of the macaque. Eur J Neurosci. 7:2064–2082.
Rockland KS. 1989. Bistratified distribution of terminal arbors of individual axons projecting from area V1 to middle temporal area (MT) in the macaque monkey. Vis Neurosci. 3:155–170.
Rockland KS. 1995. Morphology of individual axons projecting from area V2 to MT in the macaque. J Comp Neurol. 355:15–26.
Rockland KS. 2002. Non-uniformity of extrinsic connections and columnar organization. J Neurocytology. 31:247–253.
Rockland KS, Knutson T. 2001. Axon collaterals of Meynert cells diverge over large portions of area V1 in the macaque monkey. J Comp Neurol. 441:134–147.
Rockland KS, Lund JS. 1983. Intrinsic laminar lattice connections in primate visual cortex. J Comp Neurol. 216:303–318.
Salzman CD, Britten KH, Newsome WT. 1990. Cortical microstimulation influences perceptual judgements of motion direction. Nature. 346:174–177.
Sincich LC, Adams DL, Horton JC. 2003. Complete flatmounting of the macaque cerebral cortex. Vis Neurosci. 20:663–686.
Sincich LC, Blasdel GG. 2001. Oriented axon projections in primary visual cortex of the monkey. J Neurosci. 21:4416–4426.
Tanaka K, Hikosaka K, Saito H, Yukie M, Fukada Y, Iwai E. 1986. Analysis of local and wide-field movements in the superior temporal visual areas of the macaque monkey. J Neurosci. 6:134–144.
Tanigawa H, Wang Q, Fujita I. 2005. Organization of horizontal axons in the inferior temporal cortex and primary visual cortex of the macaque monkey. Cereb Cortex. 15:1887–1899.
Ungerleider LG, Mishkin M. 1979. The striate projection zone in the superior temporal sulcus of Mucaca mulatta: location and topographic organization. J Comp Neurol. 188:347–366.
Van Essen DC, Maunsell JHR, Bixby JL. 1981. The middle temporal visual area in the Macaque: Myeloarchitecture, connections, functional properties and topographic organization. J Comp Neurol. 199: 293–326.
Weller RE, Wall JT, Kaas JH. 1984. Cortical connections of the middle temporal visual area (MT) and the superior temporal cortex in owl monkeys. J Comp Neurol. 228:81–104.
Wong-Riley M. 1979. Changes in the visual system of monocularly sutured or enucleated cats demonstrable with cytochrome oxidase histochemistry. Brain Res. 171:11–28.
Xiao DK, Marcar VL, Raiguel SE, Orban GA. 1997. Selectivity of macaque MT/V5 neurons for surface orientation in depth specified by motion. Eur J Neurosci. 9:956–964.
Zeki SM. 1974a. Cells responding to changing image size and disparity in the cortex of the rhesus monkey. J Physiol (Lond). 242:827–841.
Zeki SM. 1974b. Functional organization of a visual area in the posterior bank of the superior temporal sulcus of the rhesus monkey. J Physiol (Lond). 236:549–573.
Zeki SM. 1980. The response properties of cells in the middle temporal area (area MT) of owl monkey visual cortex. Proc R Soc Lond B. 207:239–248.